MONTE CARLO STUDY OF THE PRECIPITATION KINETICS OF Al3Zr IN Al-Zr

Emmanuel Clouet, Maylise Nastar

▶ To cite this version:

MONTE CARLO STUDY
OF THE PRECIPITATION KINETICS
OF Al₃Zr IN Al-Zr

Emmanuel Clouet[1,2] and Maylise Nastar[2]

[1] Pechiney, Centre de Recherches de Voreppe
   BP 27
   38341 Voreppe cedex
   France

[2] Service de Recherches de Métallurgie Physique
   CEA/Saclay Bât. 520
   91191 Gif-sur-Yvette
   France

1. INTRODUCTION

Precipitation kinetics in alloys, like spinodal decomposition, nucleation and growth, or phase ordering, are now often studied at an atomistic scale using Monte Carlo simulations. So as to be able to reproduce the different kinetic behaviors during these transformations, one needs to adopt a realistic description of the diffusion. Therefore it is better to use a vacancy-diffusion mechanism than a direct atom exchange mechanism. It is then possible to explain why different kinetic pathways are observed. For instance, the vacancy diffusion mechanism can predict the importance of monomer diffusion with respect to the diffusion of small clusters [1, 2, 3, 4]. This leads to a difference in the cluster size distribution during precipitation [2] and determines the coarsening mechanism (evaporation-condensation or coagulation) [3, 4]. One can predict too the slowdown of precipitation kinetics by vacancy trapping due to the addition of a third component impurity [1]. Finally, different interactions of solute atoms with vacancy lead to a difference of precipitate / matrix interface morphology during the kinetic pathway, the interface being diffuse for a repulsion between vacancy and solute atoms and sharp for an attraction [4].

One drawback of kinetic Monte Carlo simulations using vacancy-diffusion mecha-

nism is that they limit themselves to pair interactions to describe configurational energy of alloys. Multisite interactions including more than two lattice sites are necessary if one wants to fully reproduce the thermodynamics of a system [5,6]. These interactions reflect dependence of bonds with their local environment and as a consequence break the symmetry imposed by pair interactions on phase diagram. It is interesting to notice that in Calphad approach [7] one naturally considers such interactions by describing formation energy of solid solutions with Redlich-Kister polynomials, and that coefficients of these polynomials can be mapped onto an Ising model to give effective interactions including more than two lattice sites [8,9]. Moreover these interactions allow one to understand shapes of precipitates in alloys [10] and can lead to a prediction of coherent interface energy in really good agreement with ab-initio calculations performed on supercells [11]. Nevertheless, to study kinetics in Monte Carlo simulations with such interactions, one usually uses a direct atom exchange mechanism [12], and thus looses all kinetic effects due to vacancy-diffusion mechanism.

We incorporate these multisite interactions in a kinetic model using a vacancy-diffusion mechanism to study precipitation kinetics of Al_3Zr in Al-Zr solid solution. For small supersaturation in zirconium of the aluminum solid solution, it has been experimentally observed that Al_3Zr precipitates are in the metastable $L1_2$ structure [13, 14, 15]. These precipitates are found to have mainly spherical shape (diameter $\sim 10 - 20$ nm), as well as rod-like shape [13]. For supersaturation higher than the peritectic concentration, nucleation is homogeneous and precipitates are coherent with the matrix [13,14]. With prolonged heat treatment, if the temperature is high enough, the metastable $L1_2$ structure can transform to the stable one DO_{23}. Using a phase field method, Proville and Finel [16] modelled these two steps of the precipitation, *i.e.* the transient nucleation of the $L1_2$ structure and the transformation to the DO_{23} structure. In this work, we only focus on the precipitation first stage, where Al_3Zr precipitates have the $L1_2$ structure and are coherent with the matrix.

We first use ab-initio calculations to fit a generalized Ising model describing thermodynamics of Al-Zr system. We then extend description of the configurational energy of the binary Al-Zr to the one of the ternary Al-Zr-Vacancy system and adopt a vacancy-atom exchange mechanism to describe kinetics. This atomistic model is used in Monte Carlo simulations to study diffusion in the Al-Zr solid solution as well as precipitation kinetics of Al_3Zr. We mainly focus our study on detecting any influence of multisite interactions on kinetics.

2.   THERMODYNAMICS OF Al-Zr BINARY

2.1.   Ab inito calculations

We use the full-potential linear-muffin-tin-orbital (FP-LMTO) method [17, 18, 19] to calculate formation energies of different compounds in the Al-Zr binary system, all based on a fcc lattice. Details of ab initio calculation can be found in appendix A. They are the same as in our previous work [20], except the fact that we use the generalized gradient approximation (GGA) instead of the local density approximation (LDA) for the exchange-correlation functional.

The use of GGA for the exchange correlation energy leads to a slightly better description of the Al-Zr system. The approximation does not fail to predict phase

stability of pure Zr [21] as LDA does: if one does not include generalized-gradient corrections, the stable structure at 0 K for Zr is found to be the ω one (hexagonal with 3 atoms per unit cell) and not the hcp structure.

Another change depending on the approximation used for the exchange-correlation functional is that formation enthalpies obtained with GGA for the different Al-Zr compounds are a little bit lower (a few percent) than with LDA. For the DO_{23} structure of Al₃Zr (table 1), GGA predicts a formation energy which perfectly reproduces the one measured by calorimetry [22]: including generalized-gradient corrections has improved the agreement. The energy of transformation from the $L1_2$ to the DO_{23} structure, $\Delta E = -23$ meV/atom, agrees really well too with the experimental one measured by Desh *et al.* [23], but this was already true with LDA. Gradient corrections have improved the agreement for the equilibrium volumes too: with the LDA, they were too low compared to the available experimental ones. Considering the values of the relaxed equilibrium parameters, shape of the unit cell and atomic positions, no change is observed according to the approximation used, both LDA and GGA being in good agreement with measured parameters.

Table 1: Calculated equilibrium volumes V_0, c'/a ratios ($c' = c/2$ for the DO_{22} phase and $c' = c/4$ for the DO_{23} phase), atomic displacements (normalized by a), and energies of formation for Al₃Zr compared to experimental data.

		V_0 (Å^3/atom)	c'/a	Atomic displacements	ΔE (eV/atom)
$L1_2$	GGA[a]	16.89			-0.478
	LDA[b]	16.12			-0.524
DO_{22}	GGA[a]	17.40	1.138		-0.471
	LDA[b]	16.60	1.141		-0.525
DO_{23}	GGA[a]	17.16	1.080	$\delta_{Al} = +0.0013$ $\delta_{Zr} = -0.0239$	-0.502
	LDA[b]	16.35	1.087	$\delta_{Al} = -0.0021$ $\delta_{Zr} = -0.0273$	-0.548
	Exp.[c]	17.25	1.0775	$\delta_{Al} = +0.0004$ $\delta_{Zr} = -0.0272$	
	Exp.[d]				-0.502 ± 0.014

[a]FP-LMTO calculations (present work)
[b]FP-LMTO calculations [20]
[c]Neutron diffraction [24]
[d]Calorimetry [22]

2.2. Cluster expansion of the formation energy

In order to express the formation energy of any Al-Zr compound based on a perfect fcc lattice, we make a cluster expansion [25] of our FP-LMTO calculations to fit a generalized Ising model. This allows us to obtain the energy of any configuration of the fcc lattice.

Considering a binary alloy of N sites on a rigid lattice, its configuration can be described through an Ising model by the vector $\boldsymbol{\sigma} = \{\sigma_1, \sigma_2, \ldots, \sigma_N\}$ where the pseudo-spin configuration variable σ_i is equal to ± 1 if an A or B atom occupies the site i. Any structure is then defined by its density matrix ρ^s, $\rho^s(\boldsymbol{\sigma})$ being the probability of finding the structure s in the configuration $\boldsymbol{\sigma}$.

With any cluster of n lattice points $\alpha = \{i_1, i_2, \ldots, i_n\}$ we associate the multisite correlation function

$$\zeta_\alpha^s = \text{Tr} \, \rho^s \prod_{i \in \alpha} \sigma_i = \frac{1}{2^N} \sum_{\boldsymbol{\sigma}} \rho^s(\boldsymbol{\sigma}) \prod_{i \in \alpha} \sigma_i, \tag{1}$$

where the sum has to be performed over the 2^N possible configurations of the lattice.

Clusters related by a translation or a symmetry operation of the point group of the structure have the same correlation functions. Denoting by D_α the number of such equivalent clusters per lattice site, or degeneracy, the energy, like any other configurational function, can be expanded in the form [25]

$$E = \sum_\alpha D_\alpha J_\alpha \zeta_\alpha^s, \tag{2}$$

where the sum has to be performed over all non equivalent clusters and the cluster interaction J_α is independent of the structure.

The cluster expansion as defined by equation 2 cannot be used directly: a truncated approximation of the sum has to be used. The truncation is made with respect to the number of points contained in a cluster, thus assuming that order effects on energy are limited to a small set of lattice points. It is truncated too with respect to distance between sites. Long range interactions are important mostly if one wants to fully reproduce elastic effects [26].

We use in the expansion of the energy six different clusters: the empty cluster $\{0\}$, the point cluster $\{1\}$, the pairs of first and second nearest neighbors $\{2,1\}$ and $\{2,2\}$, the triangle of first nearest neighbors $\{3,1\}$, and the tetrahedron of first nearest neighbors $\{4,1\}$. The corresponding cluster interactions are obtained by making a least square fit of compound energies calculated with FP-LMTO. All 17 used compounds are lying on a perfect fcc lattice: energies are calculated without any relaxation of the volume, of the shape of the unit cell, or of the atomic positions. The lattice parameter used is the one which minimizes the cohesive energy of pure Al, $a = a_{Al} = 4.044$ Å. We choose to fit the cluster expansion for the equilibrium lattice parameter of Al because we are interested in describing thermodynamics of the Al rich solid solution as well as of Al_3Zr precipitates in the $L1_2$ structure. These precipitates have an equilibrium lattice parameter close to the one of pure Al, $a = 4.073$ Å as obtained from FP-LMTO calculations with GGA, and during the nucleation stage they are coherent with the Al matrix. Consequently, such an expansion should be able to give a reasonable thermodynamic description of the different configurations reached during this precipitation stage where precipitates are coherent.

Coefficients of the cluster expansion of the energy are given in table 3. Comparing the values of the many-body interactions, we see that the main contribution to the energy arises from the pair interactions and that the 3- and 4-point cluster contributions are only corrections. Signs of pair interactions reflect the tendency of Al and Zr atoms to

Table 2: Formation energy relative to pure fcc elements for Al-Zr compounds lying on a perfect fcc lattice ($a = a_{Al} = 4.044$ Å) obtained from a direct FP-LMTO calculations and from its cluster expansion.

	Pearson symbol	Structure type	E^{form} (eV/atom) FP-LMTO	CE
Al (fcc)	cF4	Cu	0.	0.
Al$_4$Zr (D1$_a$)	tI10	MoNi$_4$	-0.421	-0.491
Al$_3$Zr (L1$_2$)	cP4	Cu$_3$Au	-0.728	-0.671
Al$_3$Zr (DO$_{22}$)	tI8	Al$_3$Ti	-0.617	-0.643
Al$_3$Zr (DO$_{23}$)	tI16	Al$_3$Zr	-0.690	-0.657
Al$_2$Zr (β)	tI6	MoSi$_2$	-0.513	-0.482
AlZr (L1$_0$)	tP4	AuCu	-0.803	-0.780
AlZr (L1$_1$)	hR32	CuPt	-0.448	-0.466
AlZr (CH40)	tI8	NbP	-0.643	-0.723
AlZr (D4)	cF32	?^{a}	-0.489	-0.414
AlZr (Z2)	tP8	?^{a}	-0.345	-0.333
Zr$_2$Al (β)	tI6	MoSi$_2$	-0.443	-0.482
Zr$_3$Al (L1$_2$)	cP4	Cu$_3$Au	-0.640	-0.603
Zr$_3$Al (DO$_{22}$)	tI8	Al$_3$Ti	-0.570	-0.574
Zr$_3$Al (DO$_{23}$)	tI16	Al$_3$Zr	-0.603	-0.589
Zr$_4$Al (D1$_a$)	tI10	MoNi$_4$	-0.390	-0.437
Zr (fcc)	cF4	Cu	0.	0.

^{a}Description of structures D4 and Z2 can be found in Ref. [6]

Table 3: Cluster expansion of the formation energy.

Cluster	D_α	J_α (eV/atom)
{0}	1	-4.853
{1}	1	0.933
{2,1}	6	97.5×10^{-3}
{2,2}	3	-28.4×10^{-3}
{3,1}	8	4.2×10^{-3}
{4,1}	2	13.1×10^{-3}

form heteroatomic first nearest neighbor pairs and homoatomic second nearest neighbor pairs.

In table 2, we compare the formation energies of the different compounds directly obtained from FP-LMTO calculations with the ones given by their cluster expansion. The standard deviation equals 41 meV/atom and the maximal difference is 79 meV/atom. This could have been improved by including more clusters in the expansion of the energy or by using a mixed-space cluster expansion [26]. Nevertheless, this would not have changed the main characteristics of the Al-Zr system, *i.e.* the short range order

tendency given by pair interactions, as well as the dependence on local environment of the interactions given by 3- and 4-point cluster interactions. In order to be able to build a realistic kinetic model and to run Monte Carlo simulations in a reasonable amount of time, we have to keep the thermodynamic description of Al-Zr system as simple as it can be. Therefore we do not try to improve expansion convergence and we focus our work on the influence of the 3- and 4-point cluster interactions on the thermodynamic and kinetic properties.
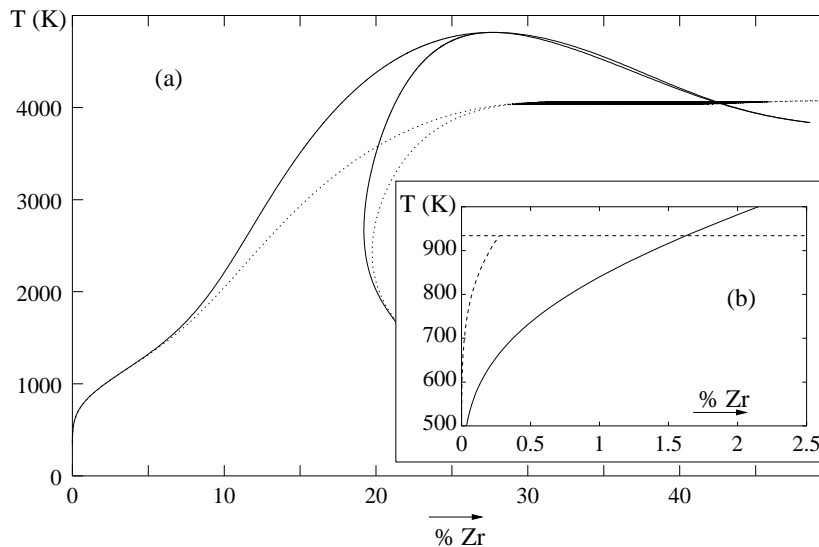
2.3. Phase diagram

Figure 1: Al rich part of the phase diagram corresponding to the equilibrium between the fcc solid solution and the $L1_2$ structure given by our set of parameters (table 3). (a) Comparison of the phase diagrams obtained with pair, triangle, and tetrahedron interactions (solid line) and the one obtained with only pair interactions (dotted line). (b) Comparison with the predicted metastable solubility limit [20] (dashed line).

We use the cluster-variation method (CVM) [27] in the tetrahedron-octahedron (TO) approximation [28, 29] to study the equilibrium between the fcc Al-rich solid solution and the $L1_2$ structure (Fig. 1) corresponding to energy parameters of table 3. At low temperature, the 2 sublattices of the $L1_2$ structure remain highly ordered, as at the experimental peritectic melting temperature ($T \sim 934$ K) the Zr concentrations of the two sublattices are respectively 100. and 1.8 at.%. Turning out the energy coefficients of the first nearest neighbor triangle and tetrahedron ($J_3 = J_4 = 0$), we see that these many-body interactions have a thermodynamic influence only at high temperature (Fig. 1 (a)), as for temperatures below 1000 K the phase diagram remains unchanged with or without these interactions.

In figure 1 (b), we compare the Zr solubility limit in the fcc solid solution corresponding to the present work energy parameters with our previous estimation of this metastable solubility limit [20]. We should point out that the solubility limit obtained with the parameters given by table 3 corresponds to a coherent equilibrium between the fcc solid solution and the $L1_2$ structure as the energy coefficients of the expansion have been calculated for a perfect fcc lattice at the parameter of pure Al. This leads to a

destabilization of the ordered phase and this is the main reason why we obtain a higher solubility than the estimated one corresponding to the equilibrium between incoherent phases. Another reason is that we use the cluster expansion to compute Al$_3$Zr cohesive energy, and thus get a small error on this energy, whereas in our previous study we directly used the value given by FP-LMTO calculation.

3. KINETIC MODEL

In order to be able to build an atomistic kinetic model, we have to generalize our thermodynamic description of the Al-Zr binary system to the one of the Al-Zr-Vacancy ternary system. To do so, we recast first the spin-like formalism of the cluster expansion into the more convenient one of the lattice gas formulation using occupation numbers [5]. This will allow us to obtain effective interactions for the different configurations of the tetrahedron of first nearest neighbors and of the pair of second nearest neighbors. Atom-vacancy interactions can then be introduced quite easily.

3.1. Effective interactions

Instead of using the pseudo-spin variables σ_n as we did in chap 2.2., this will be easier for the following to work with occupation numbers p_n^i, p_n^i being equal to 1 if an atom of type i occupies the site n and to 0 otherwise. In a binary alloy, occupation numbers and pseudo-spin variable at site n are related by

$$p_n^A = \frac{1 + \sigma_n}{2}, \qquad \text{and} \qquad p_n^B = \frac{1 - \sigma_n}{2}. \tag{3}$$

For the Al-Zr binary system, we included in our truncated cluster expansion of the energy first nearest neighbor interactions up to the pair, triangle, and tetrahedron clusters and a second nearest neighbor pair interaction. Thus, using the occupation numbers p_n^i, the expression of the energy becomes

$$E = \frac{1}{4N_s} \sum_{\substack{n,m,p,q \\ i,j,k,l}} \epsilon_{ijkl}^{(1)} p_n^i p_m^j p_p^k p_q^l + \frac{1}{2N_s} \sum_{\substack{r,s \\ i,j}} \epsilon_{ij}^{(2)} p_r^i p_s^j, \tag{4}$$

where the first sum runs over all sites (n, m, p, q) forming a first nearest neighbor tetrahedron and all their different configurations (i, j, k, l), and the second sum over all sites (r, s) forming a second nearest neighbor pair and all their different configurations (i, j). N_s is the number of lattice sites, $\epsilon_{ijkl}^{(1)}$ the effective energy of a first nearest neighbor tetrahedron in the configuration (i, j, k, l), and $\epsilon_{ij}^{(2)}$ the effective energy of a second nearest neighbor pair in the configuration (i, j).

Writing the energy with these effective interactions increases the number of dependent variables. Therefore several choices of these effective energies correspond to the same cluster expansion, then to the same thermodynamic and kinetic properties. If we make the assumption that second nearest neighbor interactions do not contribute to the cohesive energy of pure elements, *i.e.* $\epsilon_{AA}^{(2)} = 0$ and $\epsilon_{BB}^{(2)} = 0$, we obtain as many effective interactions as parameters in the truncated cluster expansion. Such an assumption does not have any physical influence and it just guarantees that homo-atomic effective interactions, $\epsilon_{AAAA}^{(1)}$ and $\epsilon_{AA}^{(2)}$, do not depend on the on the nature of B atom. Effective

energies of the first nearest neighbor tetrahedron in its different configurations are then related to the cluster expansion coefficients by the equations

$$
\begin{pmatrix}
\epsilon_{AAAA}^{(1)} \\
\epsilon_{AAAB}^{(1)} \\
\epsilon_{AABB}^{(1)} \\
\epsilon_{ABBB}^{(1)} \\
\epsilon_{BBBB}^{(1)}
\end{pmatrix}
=
\frac{1}{12}
\begin{pmatrix}
6 & 6 & 6 & 6 & 6 \\
6 & 3 & 0 & -3 & -6 \\
6 & 0 & -2 & 0 & 6 \\
6 & -3 & 0 & 3 & -6 \\
6 & -6 & 6 & -6 & 6
\end{pmatrix}
\begin{pmatrix}
D_0 J_0 + D_{2,2} J_{2,2} \\
D_1 J_1 \\
D_{2,1} J_{2,1} \\
D_{3,1} J_{3,1} \\
D_{4,1} J_{4,1}
\end{pmatrix},
\tag{5}
$$

and the second nearest neighbor pair interaction by the equation

$$
\epsilon_{AB}^{(2)} = -\frac{2}{3} D_{2,2} J_{2,2}.
\tag{6}
$$

For Al-Zr binary system, tetrahedron effective interactions corresponding to the cluster expansion of chap. 2.2. can be found in table 4: two sets are given depending if J_3 and J_4 are taken from the cluster expansion of table 3 or are supposed equal to zero. For both sets $\epsilon_{AB}^{(2)} = +0.057$ eV.

3.2.   Decomposition of effective interactions

As we wrote before, several sets of effective interactions produce the same cluster expansion. In the following, we generate the set of interactions useful for our kinetic model for which we have to count bonds we break for vacancy-atom exchange.

Different contributions are included in the effective energy $\epsilon_{ijkl}^{(1)}$. One part of the energy is due to the bonding corresponding to the six different pairs of atoms contained in the tetrahedron, each of these pairs belonging to two different tetrahedrons. Then one has to add corrections due to order on the four triangles contained in the tetrahedron and another correction due to order on the tetrahedron itself. This decomposition leads to the relation

$$
\begin{aligned}
\epsilon_{ijkl}^{(1)} \;=\;& \frac{1}{2}\left(\epsilon_{ij}^{(1)} + \epsilon_{ik}^{(1)} + \epsilon_{il}^{(1)} + \epsilon_{jk}^{(1)} + \epsilon_{jl}^{(1)} + \epsilon_{kl}^{(1)} \right) \\
& + \left(\widetilde{\epsilon}_{ijk}^{(1)} + \widetilde{\epsilon}_{ijl}^{(1)} + \widetilde{\epsilon}_{ikl}^{(1)} + \widetilde{\epsilon}_{jkl}^{(1)} \right) + \widetilde{\epsilon}_{ijkl}^{(1)},
\end{aligned}
\tag{7}
$$

where $\epsilon_{ij}^{(1)}$ is the effective energy of the first nearest neighbor pair in the configuration (i,j) and $\widetilde{\epsilon}_{ijk}^{(1)}$ and $\widetilde{\epsilon}_{ijkl}^{(1)}$ the corrections to add to pair energy due to order on triangles and on the tetrahedron

Using the previous breakdown of the tetrahedron effective energy, the expression 4 of the energy becomes

$$
\begin{aligned}
E \;=\;& \frac{1}{2N_s} \sum_{\substack{n,m \\ i,j}} \epsilon_{ij}^{(1)} p_n^i p_m^j + \frac{1}{3N_s} \sum_{\substack{n,m,p \\ i,j,k}} \widetilde{\epsilon}_{ijk}^{(1)} p_n^i p_m^j p_p^k \\
& + \frac{1}{4N_s} \sum_{\substack{n,m,p,q \\ i,j,k,l}} \widetilde{\epsilon}_{ijkl}^{(1)} p_n^i p_m^j p_p^k p_q^l + \frac{1}{2N_s} \sum_{\substack{r,s \\ i,j}} \epsilon_{ij}^{(2)} p_r^i p_s^j.
\end{aligned}
\tag{8}
$$

As this is just another mathematical way to rewrite the cluster expansion 2 of the energy, the following relations holds :

$$D_0 J_0 + D_{2,2} J_{2,2} = \frac{3}{2}\left(\epsilon_{AA}^{(1)} + 2\epsilon_{AB}^{(1)} + \epsilon_{BB}^{(1)}\right) \tag{9a}$$

$$+ \widetilde{\epsilon}_{AAA}^{(1)} + 3\widetilde{\epsilon}_{AAB}^{(1)} + 3\widetilde{\epsilon}_{ABB}^{(1)} + \widetilde{\epsilon}_{BBB}^{(1)}$$

$$+ \frac{1}{8}\left(\widetilde{\epsilon}_{AAAA}^{(1)} + 4\widetilde{\epsilon}_{AAAB}^{(1)} + 6\widetilde{\epsilon}_{AABB}^{(1)} + 4\widetilde{\epsilon}_{ABBB}^{(1)} + \widetilde{\epsilon}_{BBBB}^{(1)}\right)$$

$$D_1 J_1 = 3\left(\epsilon_{AA}^{(1)} - \epsilon_{BB}^{(1)}\right) \tag{9b}$$

$$+ 3\left(\widetilde{\epsilon}_{AAA}^{(1)} + \widetilde{\epsilon}_{AAB}^{(1)} - \widetilde{\epsilon}_{ABB}^{(1)} - \widetilde{\epsilon}_{BBB}^{(1)}\right)$$

$$+ \frac{1}{2}\left(\widetilde{\epsilon}_{AAAA}^{(1)} + 2\widetilde{\epsilon}_{AAAB}^{(1)} - 2\widetilde{\epsilon}_{ABBB}^{(1)} - \widetilde{\epsilon}_{BBBB}^{(1)}\right)$$

$$D_{2,1} J_{2,1} = \frac{3}{2}\left(\epsilon_{AA}^{(1)} - 2\epsilon_{AB}^{(1)} + \epsilon_{BB}^{(1)}\right) \tag{9c}$$

$$+ 3\left(\widetilde{\epsilon}_{AAA}^{(1)} - \widetilde{\epsilon}_{AAB}^{(1)} - \widetilde{\epsilon}_{ABB}^{(1)} + \widetilde{\epsilon}_{BBB}^{(1)}\right)$$

$$+ \frac{3}{4}\left(\widetilde{\epsilon}_{AAAA}^{(1)} - 2\widetilde{\epsilon}_{AABB}^{(1)} + \widetilde{\epsilon}_{BBBB}^{(1)}\right)$$

$$D_{3,1} J_{3,1} = \widetilde{\epsilon}_{AAA}^{(1)} - 3\widetilde{\epsilon}_{AAB}^{(1)} + 3\widetilde{\epsilon}_{ABB}^{(1)} - \widetilde{\epsilon}_{BBB}^{(1)} \tag{9d}$$

$$+ \frac{1}{2}\left(\widetilde{\epsilon}_{AAAA}^{(1)} - 2\widetilde{\epsilon}_{AAAB}^{(1)} + 2\widetilde{\epsilon}_{ABBB}^{(1)} - \widetilde{\epsilon}_{BBBB}^{(1)}\right)$$

$$D_{4,1} J_{4,1} = \frac{1}{8}\left(\widetilde{\epsilon}_{AAAA}^{(1)} - 4\widetilde{\epsilon}_{AAAB}^{(1)} + 6\widetilde{\epsilon}_{AABB}^{(1)} - 4\widetilde{\epsilon}_{ABBB}^{(1)} + \widetilde{\epsilon}_{BBBB}^{(1)}\right) \tag{9e}$$

As we want $\widetilde{\epsilon}_{ijk}^{(1)}$ to be the energetic corrections due to order on triangles, the contribution to $J_{2,1}$ of $\widetilde{\epsilon}_{AAA}^{(1)}$, $\widetilde{\epsilon}_{AAB}^{(1)}$, ... must equal zero (second term in right hand side of eq. 9c). For the same reason, the contribution to $J_{2,1}$ and $J_{3,1}$ of $\widetilde{\epsilon}_{AAAA}^{(1)}$, $\widetilde{\epsilon}_{AAAB}^{(1)}$, ... must equal zero (last term in right hand side of eq. 9c and 9d). We require too that triangle and tetrahedron order corrections do not contribute to the cohesive energy of pure elements, as we did for second nearest neighbor pair interactions. Thus, $\widetilde{\epsilon}_{AAA}^{(1)} = \widetilde{\epsilon}_{BBB}^{(1)} = 0$ and $\widetilde{\epsilon}_{AAAA}^{(1)} = \widetilde{\epsilon}_{BBBB}^{(1)} = 0$. With these restrictions, all parameters entering in the expression 8 of the energy are well determined.

The first nearest neighbor pair effective energies are thus

$$\epsilon_{AA}^{(1)} = \frac{1}{6}\left(D_0 J_0 + D_1 J_1 + D_{2,1} J_{2,1} + D_{2,2} J_{2,2} + D_{3,1} J_{3,1} + D_{4,1} J_{4,1}\right) \tag{10a}$$

$$\epsilon_{AB}^{(1)} = \frac{1}{6}\left(D_0 J_0 - D_{2,1} J_{2,1} + D_{2,2} J_{2,2} + D_{4,1} J_{4,1}\right) \tag{10b}$$

$$\epsilon_{BB}^{(1)} = \frac{1}{6}\left(D_0 J_0 - D_1 J_1 + D_{2,1} J_{2,1} + D_{2,2} J_{2,2} - D_{3,1} J_{3,1} + D_{4,1} J_{4,1}\right), \tag{10c}$$

the order corrections on first nearest neighbor triangle

$$\widetilde{\epsilon}_{AAB}^{(1)} = -\widetilde{\epsilon}_{ABB}^{(1)} = -\frac{1}{6} D_{3,1} J_{3,1}, \tag{11}$$

and the order corrections on first nearest neighbor tetrahedron

$$\widetilde{\epsilon}_{AAAB}^{(1)} = \widetilde{\epsilon}_{ABBB}^{(1)} = -D_{4,1} J_{4,1} \tag{12a}$$

$$\widetilde{\epsilon}_{AABB}^{(1)} = 0. \tag{12b}$$

Inverting the system 5, one can easily express all these quantities from the effective tetrahedron energies ϵ_{ijkl} too.

3.3. Interactions with vacancy

Within the previous formalism, we can easily introduce atom-vacancy interactions. These interactions are a simple way to take into account the electronic relaxations around the vacancy. Without them, the vacancy formation energy E_V^{for} in a pure metal would necessarily equal the cohesive energy ($E_V^{for} = 0.69$ eV [30] and $E^{coh} = 3.36$ eV for fcc Al).

We only consider first-nearest neighbor interactions with vacancies and we do not include any order correction on triangle and tetrahedron configurations containing at least one vacancy, *i.e.* $\widetilde{\epsilon}_{ijV}^{(1)} = \widetilde{\epsilon}_{ijkV}^{(1)} = 0$ where i, j, and k are any of the species Al, Zr, and V. The vacancy formation energy in a pure metal A is then given by

$$E_V^{for} = 8\epsilon_{AAAV}^{(1)} - 6\epsilon_{AAAA}^{(1)} = 12\epsilon_{AV}^{(1)} - 6\epsilon_{AA}^{(1)} \tag{13}$$

The interaction $\epsilon_{AlV}^{(1)}$ is deduced from the experimental value of the vacancy formation energy in pure Al. For the interaction $\epsilon_{ZrV}^{(1)}$, we assume that the vacancy formation energy in the fcc structure is the same as in the hcp one, these two structures being quite similar. The only experimental information we have concerning this energy is $E_V^{for} > 1.5$ eV [30]. We thus use the ab-initio value calculated by Le Bacq *et al.* [31], $E_V^{for} = 2.07$ eV. This value is calculated at the equilibrium volume of Zr and cannot be used directly to obtain $\epsilon_{ZrV}^{(1)}$ as this interaction should correspond in our model to the equilibrium lattice parameter of pure Al. We have to use instead the vacancy formation enthalpy

$$H_V^{for} = E_V^{for} + P\delta\Omega_V^{for}, \tag{14}$$

where $\delta\Omega_V^{for} = -1.164$ Å^3 is the vacancy formation volume in pure Zr [30], and P is the pressure to impose to Zr to obtain a lattice parameter equal to the one of Al. P is calculated from the bulk modulus $B = 91$ GPa of fcc Zr and the equilibrium volumes of Al and Zr, $\Omega_{Al}^0 = 16.53$ Å^3 and $\Omega_{Zr}^0 = 23.36$ Å^3, these three quantities being obtained from our FP-LMTO calculations. This gives us the value $H_V^{for} = 1.88$ eV for the vacancy formation enthalpy in pure Zr at the lattice parameter of pure Al.

We use the experimental value of the divacancy binding energy $E_{2V}^{bin} = 0.2$ eV [30] in order to compute a vacancy-vacancy interaction, $\epsilon_{VV}^{(1)} = E_{2V}^{bin} - \epsilon_{AlAl}^{(1)} + 2\epsilon_{AlV}^{(1)}$. If we do not include this interaction and set it equal to zero instead, we obtain the wrong sign for the divacancy binding energy, divacancies being thus more stable than two monovacancies. This does not affect our Monte Carlo simulations as we only include one vacancy in the simulation box, but this will have an influence if we want to build a mean field approximation of our diffusion model.

We thus managed to add vacancy contributions to our thermodynamic description of the Al-Zr binary system. Using the breakdown 7 of the first nearest neighbor tetrahedron interaction, we can obtain the effective energies corresponding to the 15 different configurations a tetrahedron can have in the ternary system. These effective energies are presented in table 4 for the cases where energy correction due to order on first nearest neighbor triangle and tetrahedron are assumed different from zero or not (J_3 and J_4 given by table 3 or $J_3 = J_4 = 0$).

Table 4: Effective energies of the first nearest neighbor tetrahedron for Al-Zr-V ternary system. The set with order correction corresponds to the values J_3 and J_4 given by the cluster expansion of table 3 and the set without order correction assumes $J_3 = J_4 = 0$.

Configuration	Effective energy (eV)	
	with order correction	without order correction
Al Al Al Al	−1.680	−1.680
Al Al Al Zr	−2.257	−2.214
Al Al Zr Zr	−2.554	−2.554
Al Zr Zr Zr	−2.707	−2.698
Zr Zr Zr Zr	−2.647	−2.647
Al Al Al V	−1.174	−1.174
Al Al Zr V	−1.567	−1.561
Al Zr Zr V	−1.748	−1.754
Zr Zr Zr V	−1.751	−1.751
Al Al V V	−0.518	−0.518
Al Zr V V	−0.758	−0.758
Zr Zr V V	−0.804	−0.804
Al V V V	+0.288	+0.288
Zr V V V	+0.194	+0.194
V V V V	+1.243	+1.243

With this set of thermodynamic parameters, we calculate the binding energy between a Zr solute atom and a vacancy in Al,

$$E_{ZrV}^{bin} = 2 \left(\epsilon_{AlAlAlAl}^{(1)} + \epsilon_{AlAlZrV}^{(1)} - \epsilon_{AlAlAlZr}^{(1)} - \epsilon_{AlAlAlV}^{(1)} \right). \tag{15}$$

The value obtained, $E_{ZrV}^{bin} = +0.369$ eV, agrees with the experimental observation that there is no attraction between Zr solute atoms and vacancies in Al [30, 32].

3.4. Migration barriers

Diffusion occurs via vacancy jumps towards one of its twelve first nearest neighbors. The vacancy exchange frequency with a neighbor of type A ($A =$Al or Zr) is given by

$$\Gamma_{A-V} = \nu_A \exp \left(-\frac{E_A^{act}}{k_B T} \right), \tag{16}$$

where ν_A is an attempt frequency and the activation energy E_A^{act} is the energy change required to move the A atom from its initial stable position to the saddle point position. It is computed as the difference between the contribution e_A^{sp} of the jumping atom to the saddle point energy and the contributions of the vacancy and of the jumping atom to the initial energy of the stable position. This last contribution is obtained by considering all bonds which are broken by the jump, $i.e.$ all pair interactions the vacancy and the jumping atoms are forming as well as all order corrections on triangles and tetrahedrons

containing the jumping atom,

$$E_A^{act} = e_A^{sp} - \sum_j \epsilon_{Vj}^{(1)} - \sum_{j \neq V} \epsilon_{Aj}^{(1)} - \sum_{jk} \widetilde{\epsilon}_{Ajk}^{(1)} - \sum_{jkl} \widetilde{\epsilon}_{Ajkl}^{(1)} - \sum_j \epsilon_{Aj}^{(2)}. \qquad (17)$$

The attempt frequency ν_A and the contribution e_A^{sp} of the jumping atom to the saddle point energy can depend on the configuration [2]. Nevertheless, we do not have enough information to see if such a dependence holds in the case of Al-Zr alloys. We thus assume that these parameters depend only on the nature of the jumping atom, which gives us four purely kinetic parameters to adjust.

The contribution of Al to the saddle point energy, e_{Al}^{sp}, is deduced from the experimental value of the vacancy migration energy in pure Al, $E_V^{mig} = 0.61$ eV [30], and the attempt frequency ν_{Al} from the experimental Al self-diffusion coefficient, $D_{Al*} = D_0 \exp{(-Q/k_B T)}$, the self-diffusion activation energy Q being the sum of the vacancy formation and migration energies in pure Al and $D_0 = 1.73 \times 10^{-5}$ m^2.s^{-1} [33].

To calculate ν_{Zr} and e_{Zr}^{sp}, we use the experimental value[1] of the diffusion coefficient of Zr impurity in Al, $D_{Zr*} = 728 \times 10^{-4} \exp{(-2.51 \text{ eV}/k_B T)}$ m^2.s^{-1} [33,34]. The kinetic parameters can be deduced from this experimental data by using the five frequency model for solute diffusion in fcc lattices [35], if we make the assumption that there is no correlation effect. We check afterwards that such an assumption is valid: at $T = 500$ K the correlation factor is $f_{Zr*} = 1$ and at $T = 1000$ K $f_{Zr*} = 0.875$. Correlation effects are thus becoming more important at higher temperature but they can be neglected in the range of temperature used in the fitting procedure.

Table 5: Kinetic parameters for a thermodynamic description of Al-Zr binary with and without energy corrections due to order on first nearest neighbor triangle and tetrahedron.

	with order correction	without order correction
e_{Al}^{sp}	-8.219 eV	-8.219 eV
e_{Zr}^{sp}	-11.286 eV	-10.942 eV
ν_{Al}	1.36×10^{14} Hz	1.36×10^{14} Hz
ν_{Zr}	4.48×10^{17} Hz	4.48×10^{17} Hz

So as to study the influence on kinetics of energy corrections due to order on triangles and tetrahedrons, we fit another set of kinetic parameters corresponding to a thermodynamic description of Al-Zr binary with only pair interactions (*i.e.* $J_3 = J_4 = 0$, or equivalently $\widetilde{\epsilon}_{ijk}^{(1)} = \widetilde{\epsilon}_{ijkl}^{(1)} = 0$). This other set of kinetic parameters presented in table 5 reproduces as well coefficients for Al self-diffusion and for Zr impurity diffusion, the only difference being that these kinetic parameters correspond to a simpler thermodynamic description of Al-Zr binary.

---

[1] Diffusion coefficient measured in the temperature range between 800 and 910 K.

4.   DIFFUSION IN SOLID SOLUTION

Diffusion in Al-Zr solid solutions can be fully characterized by the tracer correlation coefficients f_{Al} and f_{Zr} and by the phenomenological Onsager coefficients L_{AlAl}, L_{AlZr}, and L_{ZrZr}. These coefficients link fluxes of diffusing species, $\mathbf{J}_{Al}$ and $\mathbf{J}_{Zr}$, to their chemical potential gradients [36, 37] through the relations

$$\begin{aligned}
\mathbf{J}_{Al} &= -L_{AlAl}\nabla\mu'_{Al}/k_B T - L_{AlZr}\nabla\mu'_{Zr}/k_B T \\
\mathbf{J}_{Zr} &= -L_{AlZr}\nabla\mu'_{Al}/k_B T - L_{ZrZr}\nabla\mu'_{Zr}/k_B T.
\end{aligned} \tag{18}$$

Chemical potentials entering these equations are relative to the vacancy chemical potential, $\mu'_{Al} = \mu_{Al} - \mu_V$ and $\mu'_{Zr} = \mu_{Zr} - \mu_V$. We use to express diffusion fluxes the Onsager reciprocity condition, $L_{AlZr} = L_{ZrAl}$.

These coefficients can be used in finite-difference diffusion code so as to study "industrial" processes where diffusion is involved (precipitation, solidification, homogenization, ...) [38]. One way to obtain these coefficients is to adapt Calphad methodology to kinetics, *i.e.* to guess an expression for L_{AB} describing its variation with temperature and composition of the alloy and to adjust the model parameters on a large kinetic database [39, 40]. On the other hand one can use an atomistic model as the one described in chap. 3. to obtain the phenomenological coefficients [41, 8, 9]. If one carefully applies the same mean field approximation for thermodynamics and kinetics it is possible to get the whole Onsager matrix and not only diagonal terms and to catch all correlation effects [42]. Such an approach compared to the previous one does not need a huge experimental database. Moreover, as it is based on a realistic description of diffusion at the atomic scale, it appears safer to extrapolate kinetic quantities out of the range (composition or temperature) used in the fitting procedure.

In this study, we do not use any mean -field approximation to calculate phenomenological coefficients, but obtain them directly from kinetic Monte Carlo simulations by using generalization of the Einstein formula for tracer diffusion due to Allnatt [43, 37]

$$L_{AB} = \frac{\langle \mathbf{\Delta R}_A \cdot \mathbf{\Delta R}_B \rangle}{6\Delta t}, \qquad A, B = Al, Zr, \tag{19}$$

where the brackets indicate a thermodynamic ensemble average and $\mathbf{\Delta R}_A$ is the sum of total displacement $\mathbf{\Delta r}_i$ of all atoms i of type A during time Δt,

$$\mathbf{\Delta R}_A = \sum_{i \in A} \mathbf{\Delta r}_i. \tag{20}$$

We use residence time algorithm to run kinetic Monte Carlo calculations. The simulation box contains 125000 lattice sites, one of this site being occupied by a vacancy. Sum of total displacements $\mathbf{\Delta R}_{Al}$ and $\mathbf{\Delta R}_{Zr}$ in equation 19 are computed for a time interval corresponding to $\sim 10^6$ vacancy jumps, and their thermodynamic averages are obtained through simulations of 10^9 vacancy jumps. Such a big number of jumps is necessary to converge thermodynamic averages entering in the calculation of L_{AlZr} and L_{ZrZr}, whereas L_{AlAl} converges more quickly. This is due to the difference of diffusion coefficients between Al and Zr.

Results of calculations are presented in figure 2 for two different temperatures, $T = 1000$ K and $T = 900$ K, and different Zr concentration from 0 to 8 at.%. For the
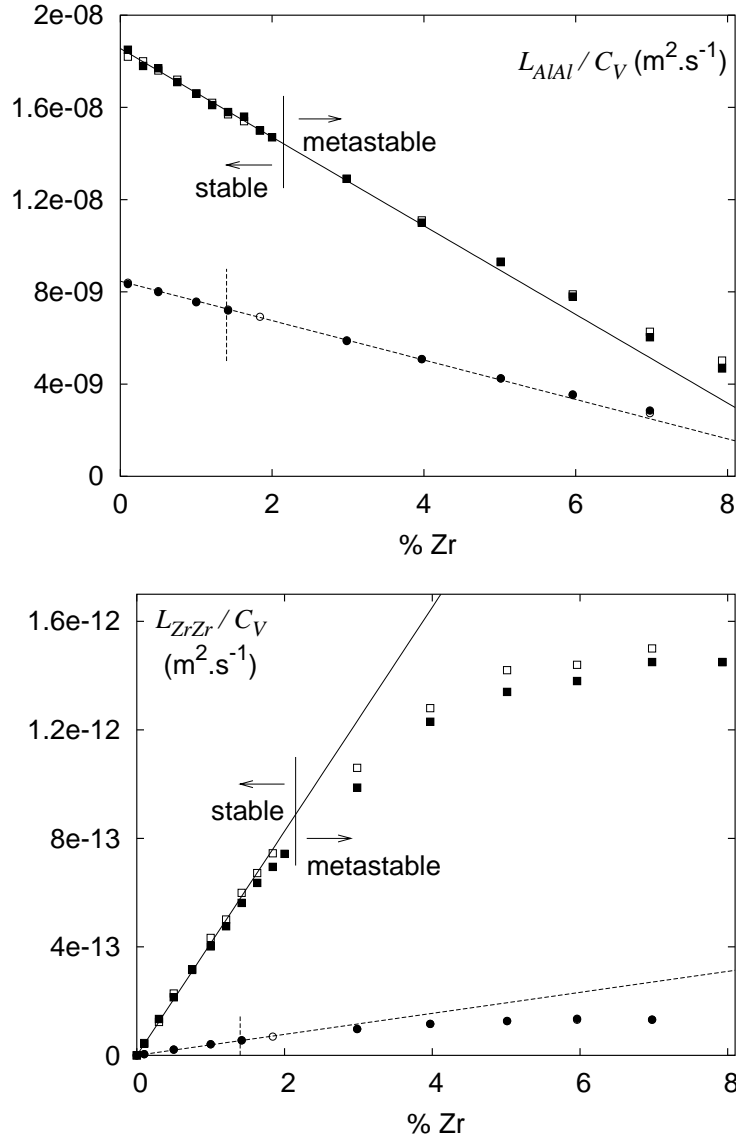
Figure 2: Onsager coefficients L_{AlAl} and L_{ZrZr}. Squares and solid lines correspond to $T = 1000$ K and circles and dashed lines to $T = 900$ K. The vertical lines indicate the corresponding solubility limit obtained from CVM calculations. Full symbols correspond to the set of parameters with order corrections on triangles and tetrahedrons and open symbols to the set without order corrections.

off-diagonal coefficient L_{AlZr} of Onsager matrix, dispersion is too important to get a precise value of thermodynamic average[2]. We interpret this as an indication that this coefficient can be neglected in this range of temperature and concentration.

Onsager coefficients are calculated for Zr concentration corresponding to the stable as well as to the metastable solid solution, the limit being given by the CVM calculations of chap. 2.2.. For calculations in the metastable solid solution, thermodynamic averages are computed during the incubation stage of precipitation kinetics when no stable precipitate is present in the simulation box (chap. 5.). L_{AlAl} behavior deviates only slightly from its linear extrapolation from the stable solid solution, but for L_{ZrZr} it

---

[2]$L_{AlZr} = 0 \pm 10^{-12}$ m^2.s^{-1} at $T = 1000$ K and $L_{AlZr} = 0 \pm 10^{-13}$ m^2.s^{-1} at $T = 900$ K

seems that no extrapolation from the stable to the metastable solid solution is possible.

So as to see the influence of triangles and tetrahedrons interactions, we ran simulations with only pair interactions considering the corresponding kinetic parameters of table 5. One can directly see on figure 2 that these two sets of parameters reproduce the same experimental data, *i.e.* the self-diffusion coefficient

$$D_{Al^*} = f_0 \lim_{C_{Zr} \to 0} L_{AlAl}, \tag{21}$$

where $f_0 = 0.78145$ for a fcc lattice, and the Zr impurity diffusion coefficient

$$D_{Zr^*} = \lim_{C_{Zr} \to 0} L_{ZrZr}/C_{Zr}. \tag{22}$$

Order corrections mainly affect L_{ZrZr}. This coefficient is slightly lower when one considers energy corrections due to order on triangles and tetrahedrons. The difference increases with Zr concentration and thus in the metastable solid solution: these order corrections lead to a slight slowdown of Zr diffusion. The two thermodynamic models are equivalent at these temperatures (*cf.* phase diagram on Fig. 1 (a)). As a consequence kinetic behaviors obtained from them are really close.
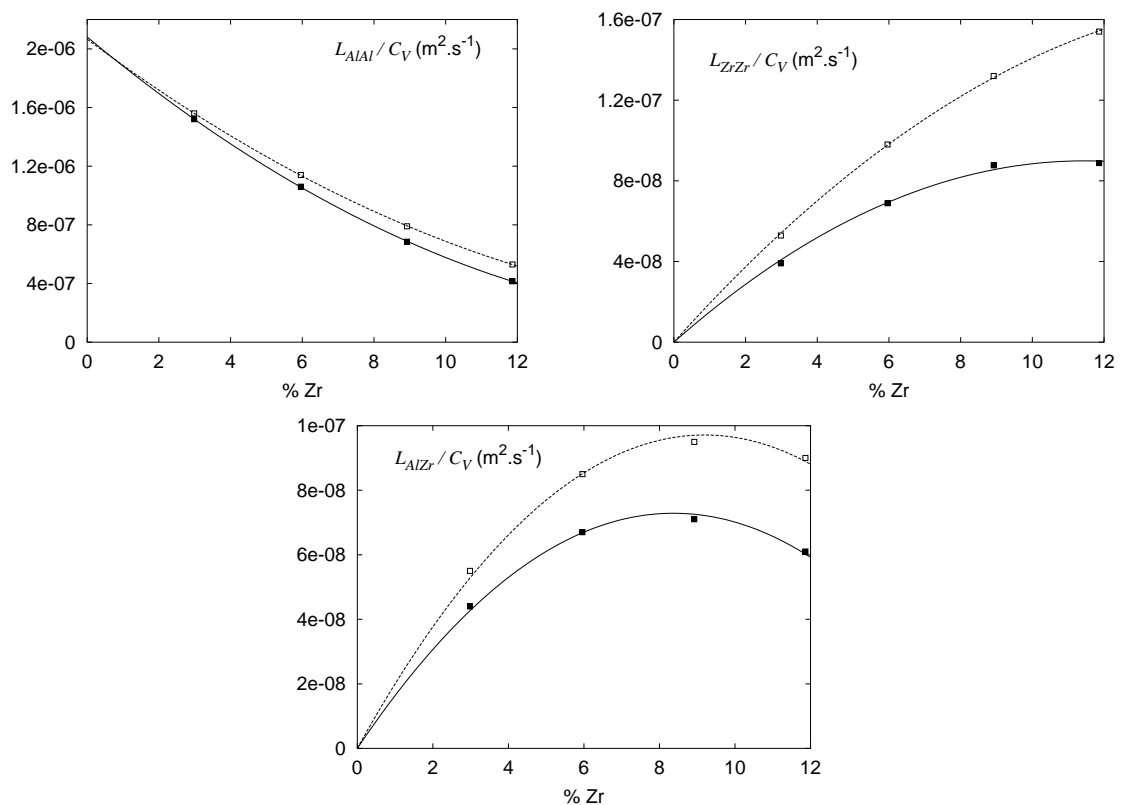

Figure 3: Onsager coefficients L_{AlAl}, L_{ZrZr}, and L_{AlZr} calculated at $T = 3000$ K. Full symbols and solid lines correspond to the set of parameters with order corrections on triangles and tetrahedrons and open symbols and dashed lines to the set without order corrections.

At higher temperatures, triangle and tetrahedron interactions change the phase diagram (Fig. 1 (a)). This thermodynamic influence leads to a kinetic change too: at

$T = 3000$ K, Onsager coefficients are lower when considering these multisite interactions (Fig. 3). One should notice that correlation effects cannot be neglected at this temperature as L_{AlZr} is far from being null. Thus one is not allowed anymore to assume Onsager matrix as diagonal. With triangle and tetrahedron interactions, Al$_3$Zr precipitate is more stable, which means that order effects are stronger. The kinetic corrolary of this thermodynamic influence is that they slow down diffusion.

5.   KINETICS OF PRECIPITATION

Precipitation kinetics have been obtained by Monte Carlo simulations for four different supersaturations of the solid solution ($C_{Zr}^0 = 5, 6, 7,$ and 8 at.%) at $T = 1000$ K. At this temperature, the equilibrium concentration is $C_{Zr}^{eq} = 2.1$ at.%. The simulation box contains 125000 lattice sites and its starting configuration is a completely disordered (random) solid solution.
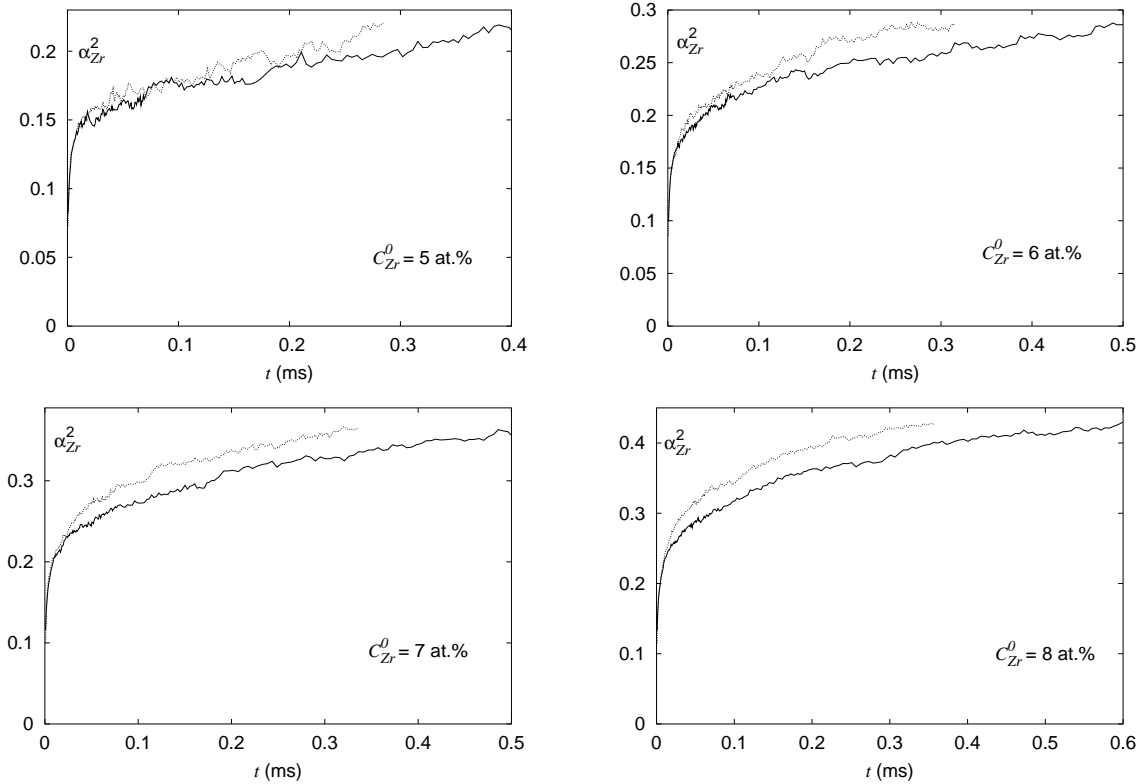
5.1.   Short range order parameters

Figure 4: Evolution of second nearest neighbor short range order of Zr atoms, α_{Zr}^2, at $T = 1000$ K and four different nominal concentrations C_{Zr}^0. Full and dotted lines are respectively for the set of parameters with and without order corrections on triangles and tetrahedrons.

The quantities of interest to follow the global evolution of precipitation during the simulation are Warren-Cowley short range order (SRO) parameters [5]. SRO parameters for first-nearest neighbors evolve too quickly to give any really significant information on precipitation state. During simulation first steps, Zr atoms surround themselves

with Al. Once this local equilibrium for first nearest neighborhood is reached, the corresponding SRO parameters do not evolve anymore. On the other hand, SRO parameters for second nearest neighbors slowly evolve until the end of the simulation. For Zr atoms, it is defined as

$$\alpha_{Zr}^2 = \frac{\langle p_n^{Zr} \rangle_{Zr,2} - C_{Zr}^0}{1 - C_{Zr}^0}, \tag{23}$$

where $\langle p_n^{Zr} \rangle_{Zr,2}$ stands for the average of occupation numbers p_n^{Zr} on all second nearest neighbors of Zr atoms. For a randomly distributed configuration of the alloy (initial configuration) $\alpha_{Zr}^2 = 0$, whereas for the L1$_2$ structure $\alpha_{Zr}^2 = 1$. Looking at fig. 4, one sees that α_{Zr}^2 evolves more quickly with the set of parameters with only pair interactions than with triangle and tetrahedron interactions. At first glance, this is in agreement with the slight difference on L_{ZrZr} measured in the metastable solid solution at this temperature (Fig. 2) for the two set of parameters. So as to see if the difference of precipitation kinetics can be understood only in terms of a difference of diffusion speed or is due to another factor, we measure the nucleation rate in our simulations and interpret it with classical theory of nucleation [44, 1, 45].

5.2. Precipitate critical size

We first need to give us a criterion to decide which atoms are belonging to L1$_2$ precipitates. As stable precipitates are almost perfectly stoichiometric at $T = 1000$ K (chap. 2.3.), we only look at Zr atoms and consider for each Zr atom in L1$_2$ precipitate that three Al atoms are belonging to the same precipitate. Zr atoms are counted as belonging to L1$_2$ precipitates if all their twelve first nearest neighbors are Al atoms and at least half of their six nearest neighbors are Zr atoms. Moreover, we impose that at least one Zr atom in a precipitate has its six second nearest neighbors being Zr, *i.e.* has a first and second nearest neighborhood in perfect agreement with the L1$_2$ structure.

Classical theory of nucleation predicts there is a critical radius, or equivalently a critical number i^* of atoms, below which precipitates are unstable and will re-dissolve into the solid solution and above which precipitates will grow. i^* is obtained by considering the competition between the interface free energy σ and the nucleation free energy per atom ΔG^n,

$$i^* = \frac{2\pi}{3} \left(\frac{a^2 \sigma}{\Delta G^n} \right)^3. \tag{24}$$

Clusters of size $i < i^*$ are considered to be local variations of the solid solution composition and thus are not counted as L1$_2$ precipitates.

5.3. Nucleation free energy

The nucleation free energy per atom entering equation 24 is given by [44, 45]

$$\Delta G^n = \frac{3}{4} \left(\mu_{Al}(C_{Zr}^{eq}) - \mu_{Al}(C_{Zr}^0) \right) + \frac{1}{4} \left(\mu_{Zr}(C_{Zr}^{eq}) - \mu_{Zr}(C_{Zr}^0) \right), \tag{25}$$

where $\mu_{Al}(C_{Zr})$ and $\mu_{Zr}(C_{Zr})$ are the chemical potentials of respectively Al and Zr components in the solid solution of concentration C_{Zr}, C_{Zr}^{eq} is the equilibrium concentration of the solid solution, and C_{Zr}^0 the nominal concentration. The factors 3/4 and 1/4
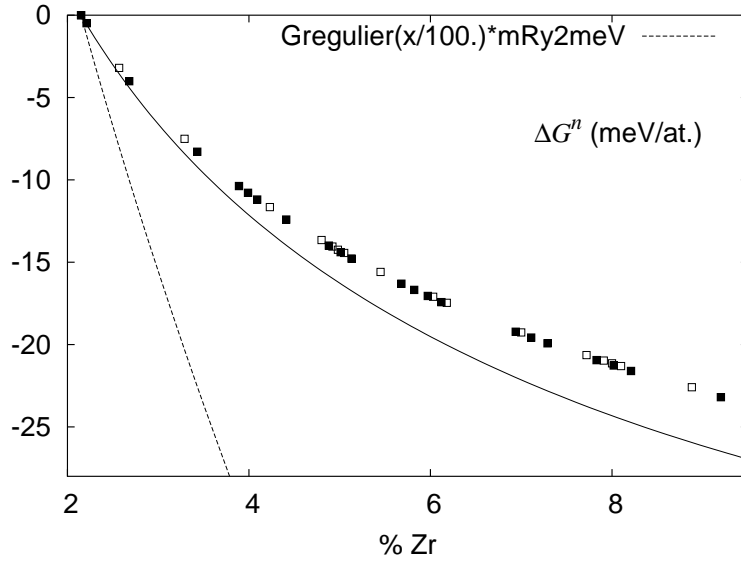
Figure 5: Nucleation free energy ΔG^n at $T = 1000$ K for different concentration of the solid solution. Square symbols correspond to CVM-TO calculation and the line to the ideal solution approximation (eq. 26). Full and open symbols are respectively for the set of parameters with and without order corrections on triangles and tetrahedrons.

arises from the stoichiometry of the precipitating phase Al_3Zr. Usually the nucleation free energy is approximated by

$$\Delta G^n = \frac{3}{4}k_B T \log \frac{1 - C_{Zr}^{eq}}{1 - C_{Zr}^0} + \frac{1}{4}k_B T \log \frac{C_{Zr}^{eq}}{C_{Zr}^0} \tag{26}$$

which is obtained by considering in equation 25 the expressions of the chemical potentials for an ideal solution. As at $T = 1000$ K we obtained the same solubility limit, $C_{Zr}^{eq} = 2.1$ at.%, with or without triangle and tetrahedron interactions (cf. phase diagram on fig. 1), the approximation 26 cannot be used to see if these interactions have any influence on the nucleation free energy. Therefore we use CVM-TO to calculate chemical potentials entering expression 25. Looking at figure 5, one should notice that the ideal solution approximation would have lead to an overestimation of ΔG^n, the error being $\sim 10\%$ for the maximal supersaturation considered. With CVM-TO, we do not obtain any change in the value of the nucleation free energy depending we are considering or not order corrections for first nearest neighbor triangle and tetrahedron. Thus slowdown of precipitation kinetics with these corrections cannot be explained by a decreasing of the nucleation free energy.

5.4. Interface free energy

To determine the precipitate critical size i^* using expression 24, we need to know the value of the interface free energy σ too. We calculate this energy at 0 K for different orientations of the interface. We therefore do not consider any configurational entropy and simply obtain the interface energy by counting the number by area unit of wrong "bonds" compared to pure Al and Al_3Zr in $L1_2$ structure. For (100) and (110) interfaces there is an ambiguity in calculating such an energy as two different

planes, one pure Al and the other one of stoichiometry Al$_{1/2}$Zr$_{1/2}$, can be considered as interface. Considering L1$_2$ precipitates as stoichiometric will guarantee that to any type of the two possible interfaces is associated a parallel interface of the other type. Thus for (100) and (110) interfaces, we consider the average of these two different interface energies to be meaningful for the parameter σ entering in classical theory of nucleation. For (111) interface, as only one interface of stoichiometry Al$_{3/4}$Zr$_{1/4}$ is possible, we do not obtain such an ambiguity. The energies corresponding to these different interfaces are

$$\sigma_{100} = \frac{1}{\sqrt{2}}\sigma_{110} = \frac{1}{\sqrt{3}}\sigma_{111} = \frac{2\epsilon_{AB}^{(2)} - \epsilon_{AA}^{(2)} - \epsilon_{BB}^{(2)}}{2a^2}, \quad \text{with} \quad a^2\sigma_{100} = 57.0 \text{ meV}.$$

These interface energies only depend on second nearest neighbor interactions and therefore are the same with or without order corrections on first nearest neighbor triangle and tetrahedron. To determine the critical size of precipitates with equation 24 we use an interface free energy slightly higher than σ_{100}, $a^2\sigma = 64.1$ meV. With this interface free energy, nucleation rate obtained from Monte Carlo simulations are in better agreement than with σ_{100} (Fig. 7). As precipitates observed in Monte Carlo simulations do not exhibit sharp interfaces, this is quite natural to have to use an energy higher than the minimal calculated one.

5.5. Nucleation rate

Critical size for precipitates obtained from these nucleation and interface free energies are respectively $i^* = 187$, 104, 76, and 57 atoms for the different nominal concentrations $C_{Zr}^0 = 5$, 6, 7, and 8 at.%. We use these critical sizes to determine the number N_p of supercritical precipitates contained in the simulation boxes, their average size $\langle i \rangle_p$, as well as the concentration of the solid solution C_{Zr}. The variation with time of these quantities are shown on fig. 6 for the simulation box of nominal concentration $C_{Zr}^0 = 8$ at.%. After an incubation time, one observes a nucleation stage where the number of precipitates increases linearly until it reaches a maximum. We then enter into the growth stage: the number of precipitates does not vary and their size is increasing. At last, during the coarsening stage, precipitates are still growing but their number is decreasing. For this concentration, one clearly sees that precipitation kinetics is faster with only pair interactions as the number of precipitates is increasing more rapidly. Moreover precipitates have a bigger size than with triangle and tetrahedron order corrections.

The steady-state nucleation rate J^{st} is measured during the nucleation stage, when the number of precipitates is varying quite linearly with time. Slowdown of precipitation kinetics with triangle and tetrahedron order corrections can be seen on the steady-state nucleation rate (Fig. 7): without these corrections J^{st} is about two times higher than when these corrections are included.

In classical theory of nucleation, the steady-state nucleation rate is given by the expression [44],

$$J^{st} = N_0 Z\beta^* \exp{-\frac{\Delta G^*}{kT}}, \tag{27}$$

where N_0 is the number of nucleation sites, *i.e.* the number of lattice sites ($N_0 = 125000$ for Monte Carlo simulations), ΔG^* is the nucleation barrier and corresponds to the free
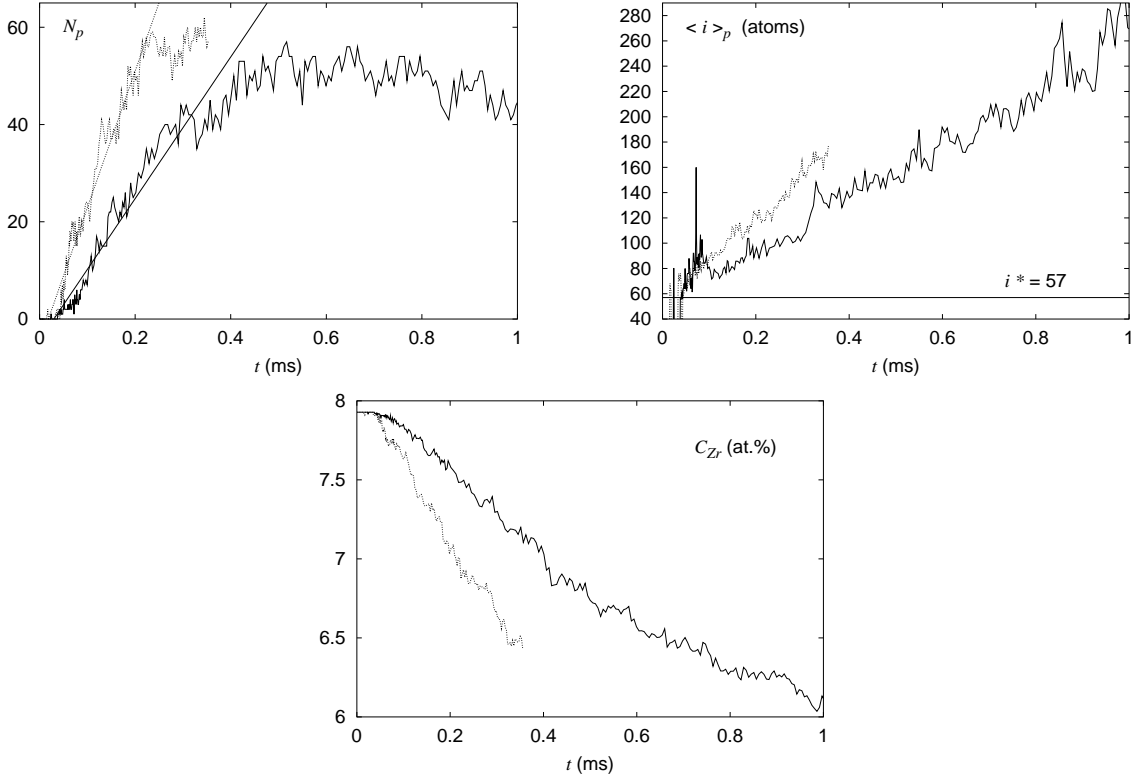
Figure 6: Kinetics of precipitation for a nominal Zr concentration $C_{Zr}^0 = 8$ at.%: evolution with time of the number N_p of precipitates in the simulation box, of precipitates average size $< i >_p$, and of Zr concentration in the solid solution. Full and dotted lines are respectively for the set of parameters with and without order corrections on triangles and tetrahedrons.

energy of a precipitate of critical size i^*,

$$\Delta G^* = \frac{\pi}{3} \frac{(a^2 \sigma)^3}{\Delta G^{n2}}, \tag{28}$$

Z is the Zeldovitch factor and describes size fluctuations of precipitates around i^*,

$$Z = \frac{1}{2\pi} \frac{\Delta G^{n2}}{(a^2 \sigma)^{3/2} \sqrt{kT}}, \tag{29}$$

and β^* is the condensation rate for clusters of critical size i^*. Assuming the limiting step of the adsorption is the long range diffusion of Zr atoms in the solid solution, the condensation rate is [44]

$$\beta^* = 8\pi \frac{a^2 \sigma}{\Delta G^n} \frac{D_{Zr}}{a^2} C_{Zr}^0. \tag{30}$$

Zr diffusion coefficient is obtained from our measure of Onsager coefficients in the metastable solid solution (chap. 4.). Assuming that vacancies are at equilibrium ($\mu_V = 0$), its expression is [35, 36, 37]

$$D_{Zr} = \left(L_{ZrZr} - \frac{C_{Zr}^0}{1 - C_{Zr}^0} L_{AlZr} \right) \frac{1}{k_B T} \frac{\partial \mu_{Zr}}{\partial C_{Zr}^0} \tag{31}$$
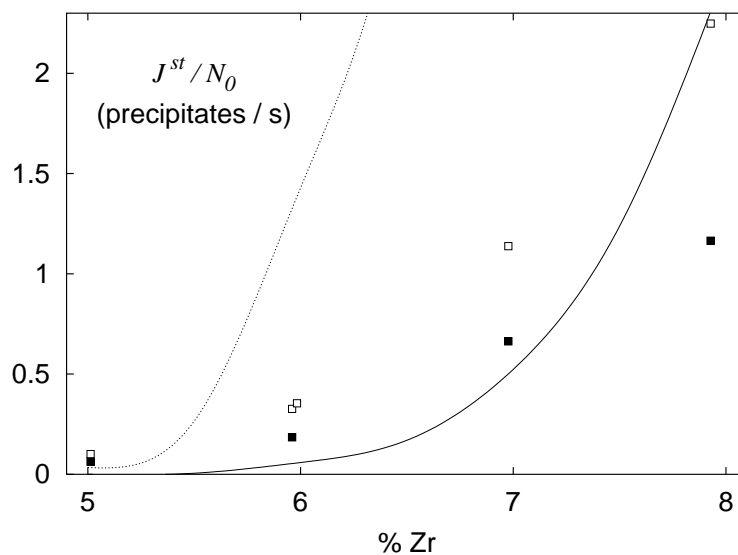
Figure 7: Evolution of the steady-state nucleation rate J^{st} with the nominal concentration for $T = 1000$ K. Full and open symbols are respectively for the set of parameters with and without order corrections on triangles and tetrahedrons. The full line corresponds to the nucleation rate predicted by classical theory of nucleation with $a^2\sigma = 64.1$ meV and the dotted line with $a^2\sigma = a^2\sigma_{100} = 57.0$ meV. J^{st} is normalized by the number of lattice sites in the simulation box, $N_0 = 125000$.

We obtain the thermodynamic factor $\partial\mu_{Zr}/\partial C^0_{Zr}$ using CVM-TO calculations. This factor is the same with or without order corrections on triangles and tetrahedrons. Therefore, the only difference these corrections induce on Zr diffusion arises from L_{ZrZr}. In classical theory of nucleation, the diffusion coefficient entering in the expression 30 of the condensation rate is only a scaling factor for time and does not have any other influence on kinetics. As a consequence the steady-state nucleation rate varies linearly with Zr diffusion coefficient as it clearly appears when combining equations 30 and 27. Thus small variations of L_{ZrZr} with the set of parameters used do not allow to explain the difference of the nucleation rate: with order corrections, L_{ZrZr} is far from being half the value it is with only pair interactions (Fig. 2). Thus slowdown of precipitation kinetics is not due to a slowdown of Zr diffusion.

One possible explanation would be a difference of the interface free energy σ. J^{st} is really sensitive to this parameter and one only needs a small decrease of σ to obtain a higher nucleation rate (see on fig. 7 the decrease of J^{st} when $a^2\sigma$ is going from 57.0 to 64.1 meV). Such a decrease would explain too why precipitates have a bigger size with only pair interactions. At $T = 0$ K, we obtain the same interface energy for all directions considered with the two sets of parameters, but at finite temperature the configurational entropy could lead to a difference of interface free energy. Nevertheless, this needs to be confirmed, by CVM calculations or using the Cahn-Hilliard method [46] for instance. Another possible explanation to understand the different kinetic pathways would be a different mobility of small clusters with the two sets of parameters. But this would be quite surprising, as we do not expect small clusters to be really mobile because of the repulsion between vacancy and Zr solute atoms.

6. CONCLUSIONS

We built an atomistic kinetic model for Al-Zr binary system using ab-initio calculations as well as experimental data. So as to be as realistic as it should be at this atomic scale, this model describes diffusion through vacancy jumps. Thanks to ab-initio calculations we could improve usual thermodynamic descriptions based on pair interactions and incorporate multisite interactions for clusters containing more than two lattice points so as to consider dependence of bonds with their local environment.

At temperatures lower than 1000 K, these energetic corrections due to local order do not modify thermodynamics: the phase diagram does not change when one does not consider these order corrections. For higher temperatures they lead to a stabilization of the ordered structure L1$_2$.

Concerning diffusion in the solid solution, these order corrections on first nearest neighbor triangle and tetrahedron do not really change the Onsager matrix, and thus diffusion characteristics. They just lead to a slight slowdown of Zr diffusion in the metastable solid solution. When looking at higher temperatures, the slowdown of Zr diffusion is more important.

For precipitation, kinetics are slower with these interactions. The slowdown is too important to be related to the small decrease of Zr diffusion in the metastable solid solution at the same temperature. One possibility would be a change of configurational entropy contribution to interface free energy.

A   DETAILS OF AB-INITIO CALCULATIONS

Ab initio calculations were carried out using a full-potential linear-muffin-tin-orbital (FP-LMTO) method [17, 18, 19] in the version developed by Methfessel and Van Schilfgaarde [47]. The basis used contained 22 energy independent muffin-tin-orbitals (MTO) per Al and Zr site: three κ values for the orbitals s and p and two κ values for the orbitals d where the corresponding kinetic energies were $\kappa^2 = 0.01$ Ry (spd), 1.0 Ry (spd), and 2.3 Ry (sp). A second panel with a basis composed of 22 energy independent MTO with the same kinetic energies was used to make a correct treatment of the 4p semicore states of Zr. The same uniform mesh of points was used to make the integrations in the Brillouin zone for valence and semicore states. The radii of the muffin-tin spheres were chosen to have a compactness of 47.6% for Al sites and 54.1% for Zr sites. Inside the muffin-tin spheres, the potential is expanded in spherical harmonics up to $l = 6$ and in the interstitial region spherical Hankel functions of kinetic energies $\kappa^2 = 1$ Ry and 3.0 Ry were fitted up to $l = 6$. The calculations were performed in the generalized

gradient approximation (GGA) [48, 49] and the parameterization used was the one of Perdew *et al.* [50].

References

[1] F. Soisson and G. Martin, "Monte-Carlo simulations of the decomposition of metastable solid solutions: Transient and steady-state nucleation kinetics," *Phys. Rev. B*, vol. 62, pp. 203–214, 2000.

[2] Y. Le Bouar and F. Soisson, "Kinetics pathway from embedded-atom-method potential: Influence of the activation barriers," *Phys. Rev. B*, vol. 65, p. 0914103, 2002.

[3] M. Athènes, P. Bellon, and G. Martin, "Effects of atomic mobilities on phase separation kinetics: a Monte-Carlo study," *Acta mater.*, vol. 48, pp. 2675–2688, 2000.

[4] J. M. Roussel and P. Bellon, "Vacancy-assisted phase separation with asymmetric atomic mobility: Coarsening rates, precipitate composition, and morphology.," *Phys. Rev. B*, vol. 63, p. 184114, 2001.

[5] F. Ducastelle, *Order and Phase Stability in Alloys.* North-Holland, Amsterdam, 1991.

[6] Z. W. Lu, S.-H. Wei, A. Zunger, S. Frota-Pessoa, and L. G. Ferreira, "First-principles statistical mechanics of structural stability of intermetallic compounds," *Phys. Rev. B*, vol. 44, pp. 512–544, 1991.

[7] N. Saunders and A. P. Miodownik, *CALPHAD – Calculation of Phase Diagrams – A Comprehensive Guide.* Oxford: Pergamon, 1998.

[8] C. Desgranges, F. Deffort, S. Poissonet, and G. Martin, "Interdiffusion in concentrated quaternary Ag-In-Cd-Sn alloys: Modelling and measurements," in *Defect and Diffusion Science Forum*, vol. 143–147, pp. 603–608, 1997.

[9] C. Desgranges, *Compréhension et Prédiction du Comportement sous Irradiation Neutronique d'Alliages Absorbants à Base d'Argent.* PhD thesis, Université Paris XI Orsay, 1998.

[10] S. Müller, C. Wolverton, L.-W. Wang, and A. Zunger, "Prediction of alloy precipitate shapes from first principles," *Europhysics Letters*, vol. 55, pp. 33–39, 2001.

[11] M. Asta, S. M. Foiles, and A. A. Quong, "First-principles calculations of bulk and interfacial thermodynamic properties for fcc-based Al-Sc alloys," *Phys. Rev. B*, vol. 57, no. 18, pp. 11265–11275, 1998.

[12] S. Müller, L.-W. Wang, and A. Zunger, "First-principles kinetics theory of precipitate evolution in Al-Zn," *Modelling Simul. Mater. Sci. Eng.*, vol. 10, pp. 131–145, 2002.

[13] N. Ryum, "Precipitation and recrystallization in an Al-0.5 wt.% Zr alloy," *Acta Metall.*, vol. 17, pp. 269–278, 1969.

[14] J. D. Robson and P. B. Prangnell, "Dispersoid precipitation and process modelling in zirconium containing commercial aluminium alloys," *Acta Mater.*, vol. 49, pp. 599–613, 2001.

[15] E. Nes, "Precipitation of the metastable cubic Al$_3$Zr-phase in subperitectic Al-Zr alloys," *Acta Metall.*, vol. 20, pp. 499–506, 1972.

[16] L. Proville and A. Finel, "Kinetics of the coherent order-disorder transion in Al$_3$Zr," *Phys. Rev. B*, vol. 64, p. 054104, 2001.

[17] O. K. Andersen, "Linear methods in band theory," *Phys. Rev. B*, vol. 12, no. 8, pp. 3060–3083, 1975.

[18] M. Methfessel, "Elastic constants and phonon frequencies of Si calculated by a fast full-potential LMTO method," *Phys. Rev. B*, vol. 38, no. 2, pp. 1537–1540, 1988.

[19] M. Methfessel, C. O. Rodriguez, and O. K. Andersen, "Fast full-potential calculations with a converged basis of atom-centered linear muffin-tin orbitals: Structural and dynamic properties of silicon," *Phys. Rev. B*, vol. 40, no. 3, pp. 2009–2012, 1989.

[20] E. Clouet, J. M. Sanchez, and C. Sigli, "First-principles study of the solubility of Zr in Al," *Phys. Rev. B*, vol. 65, p. 094105, 2002.

[21] G. Jomard, L. Magaud, and A. Pasturel, "Full-potential calculations using the generalized-gradient corrections: Structural properties of Ti, Zr and Hf under compression," *Philos. Mag. B*, vol. 77, no. 1, pp. 67–74, 1998.

[22] S. V. Meshel and O. J. Kleppa, "Standard enthalpies of formation of 4d aluminides by direct synthesis calorimetry," *J. Alloys Compd.*, vol. 191, pp. 111–116, 1993.

[23] P. B. Desch, R. B. Schwarz, and P. Nash, "Formation of metastable L1$_2$ phases in Al$_3$Zr and Al-12.5%X-25%Zr (X≡Li, Cr, Fe, Ni, Cu)," *J. Less-Common Metals*, vol. 168, pp. 69–80, 1991.

[24] C. Amador, J. J. Hoyt, B. C. Chakoumakos, and D. de Fontaine, "Theoretical and experimental study of relaxation in Al$_3$Ti and Al$_3$Zr ordered phases," *Phys. Rev. Lett.*, vol. 74, no. 24, pp. 4955–4958, 1995.

[25] J. M. Sanchez, F. Ducastelle, and D. Gratias, "Generalized cluster description of multicomponent systems," *Physica*, vol. A 128, pp. 334–350, 1984.

[26] D. B. Laks, L. G. Ferreira, S. Froyen, and A. Zunger, "Efficient cluster expansion for substitutional systems," *Phys. Rev. B*, vol. 46, no. 19, pp. 12587–12605, 1992.

[27] R. Kikuchi, "A theory of cooperative phenomena," *Phys. Rev.*, vol. 81, no. 6, pp. 988–1003, 1951.

[28] J. M. Sanchez and D. de Fontaine, "Ordering in fcc lattices with first- and second-neighbor interactions," *Phys. Rev. B*, vol. 21, p. 216, 1980.

[29] T. Mohri, J. M. Sanchez, and D. de Fontaine, "Binary ordering prototype phase diagrams in the cluster variation approximation," *Acta Met.*, vol. 33, pp. 1171–85, 1985.

[30] P. Ehrhart, P. Jung, H. Schultz, and H. Ullmaier, "Atomic defects in metals," in *Landolt-Börnstein, New Series, Group III* (H. Ullmaier, ed.), vol. 25, Berlin: Springer-Verlag, 1991.

[31] O. Le Bacq, F. Willaime, and A. Pasturel, "Unrelaxed vacancy formation energies in group-IV elements calculated by the full-potential linear muffin-tin orbital method: Invariance with crystal structure," *Phys. Rev. B*, vol. 59, pp. 8508–8515, 1999.

[32] J. P. Simon, "Étude par trempe des interactions lacunes-impuretés dans les alliages dilués Al-Zr et Al-Cr," *Phys. Stat. Sol. (a)*, vol. 41, p. K107, 1977.

[33] H. Bakker, H. P. Bonzel, C. M. Bruff, M. A. Dayananda, W. Gust, J. Horvth, I. Kaur, G. Kidson, A. D. LeClaire, H. Mehrer, G. Murch, G. Neumann, N. Stolica, and N. A. Stolwijk, "Diffusion in solid metals and alloys," in *Landolt-Börnstein, New Series, Group III* (H. Mehrer, ed.), vol. 26, Berlin: Springer-Verlag, 1990.

[34] T. Marumo, S. Fujikawa, and K. Hirano, "Diffusion of zirconium in aluminum," *Keikinzoku - J. Jpn. Inst. Light Met.*, vol. 23, p. 17, 1973.

[35] J. L. Bocquet, G. Brebec, and Y. Limoge, "Diffusion in metals ans alloys," in *Physical Metallurgy* (R. W. Cahn and P. Haasen, eds.), ch. 7, pp. 536–668, Amsterdam: North-Holland, 1996.

[36] J. Philibert, *Atom Movements - Diffusion and Mass Transport in Solids.* Les Ulis, France: Les éditions de physique, 1991.

[37] A. R. Allnatt and A. B. Lidiard, *Atomic Transport in Solids.* Cambridge University Press, 1993.

[38] A. Borgenstam, A. Engström, L. Höglund, and J. Agren, "DICTRA, a tool for simulation of diffusional transformations in alloys," *J. Phase Equil.*, vol. 21, pp. 269–280, 2000.

[39] J.-O. Andersson and J. Ågren, "Models for numerical treatment of multicomponent diffusion in simple phases," *J. Appl. Phys.*, vol. 72, pp. 1350–1355, 1992.

[40] C. E. Campbell, W. J. Boettinger, and U. R. Kattner, "Development of a diffusion mobility database for Ni-base superalloys," *Acta Mat.*, vol. 50, pp. 775–792, 2002.

[41] G. Martin, "Atomic mobility in Cahn's diffusion model," *Phys. Rev. B*, vol. 41, p. 2279, 1990.

[42] M. Nastar, V. Y. Dobretsov, and G. Martin, "Self-consistent formulation of configurational kinetics close to equilibrium: the phenomenological coefficients for diffusion in crystalline solids," *Phil. Mag. A*, vol. 80, p. 155, 2000.

[43] A. R. Allnatt, "Einstein and linear response formulae for the phenomenological coefficients for isothermal matter transport in solids," *J. Phys. C: Solid State Phys.*, vol. 15, pp. 5605–5613, 1982.

[44] G. Martin, "The theories of unmixing kinetics of solid solutions," in *Solid State Phase Transformation in Metals and Alloys*, (Orsay, France), pp. 337–406, Les Éditions de Physique, 1978.

[45] D. A. Porter and K. E. Easterling, *Phase Transformations in Metals and Alloys*. London: Chapman & Hall, 1992.

[46] J. W. Cahn and J. Hilliard, "Free energy of a nonuniform system. interface free energy," *J. Chem. Phys.*, vol. 28, pp. 258–267, 1958.

[47] M. Methfessel and M. van Schilfgaarde, "Derivation of force theorem in density-functional theory: Application to the full-potential LMTO method," *Phys. Rev. B*, vol. 48, no. 7, pp. 4937–4940, 1993.

[48] P. Hohenberg and W. Kohn, "Inhomogeneous electron gas," *Phys. Rev.*, vol. 136, no. 3B, pp. B864–B871, 1964.

[49] W. Kohn and L. J. Sham, "Self-consistent equations including exchange and correlations effects," *Phys. Rev.*, vol. 140, no. 4A, pp. A1133–A1138, 1965.

[50] J. P. Perdew, K. Burke, and M. Ernzerhof, "Generalized gradient approximation made simple," *Phys. Rev. Lett.*, vol. 77, no. 18, pp. 3865–3868, 1996.